An untethered magnetic- and light-responsive rotary gripper: shedding light on photoresponsive liquid crystal actuators

Please check the document version of this publication:

An Untethered Magnetic- and Light-Responsive Rotary Gripper: Shedding Light on Photoresponsive Liquid Crystal Actuators

Marina Pilz da Cunha, Yari Foelen, Roel J. H. van Raak, Jeffrey N. Murphy, Tom A. P. Engels, Michael G. Debije, and Albert P. H. J. Schenning*

Here, a remotely controlled dual magneto- and photoresponsive soft robotic gripper is reported, capable of loading, transport, rotation, and release of cargo. The untethered soft actuator consists of a magnetically responsive polydimethylsiloxane layer containing magnetic iron powder coated onto the central region of a light-responsive liquid crystal polymer film hosting photochromic azobenzene dyes. Light is used to trigger the actuator to autonomously grab and pick up cargo with a high degree of control. Magnetic response is employed to conduct the locomotion as magnetic guidance, allowing the gripper to have both translational freedom and rotational freedom in its locomotion, differentiating the device from other soft robotic grippers. Control can be attained even in enclosed and/or confined spaces, through solely remote actuation. Through combined video, mechanical, and thermal analyses, the actuation mechanism of the light-responsive liquid crystal network is investigated, shedding light on the decisive role of the temperature evolution in governing both rate of motion and deformation amplitude of the light-responsive soft actuator.

1. Introduction

Nature's array of stimuli-responsive systems and organisms remain a constant source of inspiration for scientists in the development of soft actuators. Stimuli-responsive materials exhibiting remotely powered actuation have potential applications in a variety of fields, ranging from soft/microrobotics,[1–4] energy generation,[5] microfluidic,[6] and medical devices.[7,8] Moreover, the integration of multitriggered responsive actuation into single devices is of interest for the next-generation smart

materials and is desired for untethered multi-responsive soft robotics, opening a new range of applications, expanding from remotely controlled motion to possible locomotion. However, a facile approach to combining multi-stimulus response into one device without imposing dramatic mechanical or chemical changes to the system remains a challenge. Grasping devices making use of stimuli-responsive actuation have already been reported[9–15] and a present goal in this field is to free these stimuli-responsive soft robotic grippers from the necessity of manual manipulation for movement.

Combining soft materials and stimuli-responsive reagents for the development of functional materials is a present endeavor.[16] Liquid crystal networks (LCNs) are attractive materials for fabricating soft actuators since they operate in dry environments, and their deformation can be programmed within the LC network by the 3D organization of the molecular building blocks. The versatility of liquid crystal (LC) networks has allowed for the development of several functional, responsive actuators with diverse fabrication techniques, such as 3D printing,[17] and operating with a variety of triggers, including light,[18–22] heat,[23] humidity,[24,25] and magnetic,[26,27] and electric[28] fields. Among the triggers studied in the development of LC actuators, light is highly appealing for untethered motion as it provides instantaneous stimulus, resulting in a fast response

M. Pilz da Cunha, Y. Foelen, R. J. H. van Raak, Dr. J. N. Murphy,
Dr. M. G. Debije, Prof. A. P. H. J. Schenning
Laboratory of Stimuli-Responsive Functional Materials & Devices
Department of Chemical Engineering and Chemistry
Eindhoven University of Technology
P.O. Box 513, 5600 MB Eindhoven, The Netherlands
E-mail: a.p.h.j.schenning@tue.nl

The ORCID identification number(s) for the author(s) of this article
can be found under https://doi.org/10.1002/adom.201801643.

M. Pilz da Cunha, Prof. A. P. H. J. Schenning
Institute for Complex Molecular Systems
Eindhoven University of Technology
Den Dolech 2, 5600 MB Eindhoven, The Netherlands

Dr. T. A. P. Engels
Department of Mechanical Engineering
Materials Technology Institute
Eindhoven University of Technology
P.O. Box 513, 5600 MB Eindhoven, The Netherlands

Prof. A. P. H. J. Schenning
SCNU-TUE Joint Laboratory of Device
Integrated Responsive Materials (DIRM)
South China Normal University
Guangzhou Higher Education Mega Center
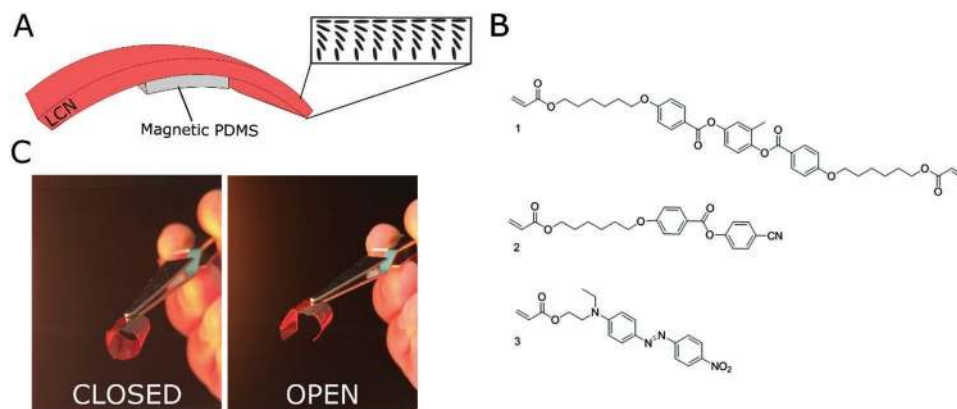510006 Guangzhou, China

Figure 1. A) Magneto and light-responsive actuator designs, with localized PDMS/Fe composite layer coated on a section of the homeotropic side of the splay-aligned LCN. B) Chemical structures of monomers used in making the LCN, with azobenzene derivative **3** as the light-responsive dye. C) Photograph of the LCN soft gripper (16 mm in length by 9 mm in width; the PDMS/iron layer is 120 µm thick) in the closed state and open state after light exposure.

with a high degree of control. Many different light-responsive LCNs have been reported, of which most contain photochromic azobenzenes. Although several works in the literature distinguish and describe mechanisms underlying photoinduced actuation of photochromic azobenzene-doped LCNs,[29–35] the connection between isomerization, photosoftening, and heating timescales with the macroscopic deformation, considering both actuation rates and equilibrium conditions, remains concealed. Understanding of the interplay of the molecular processes, mechanical actions and actuating properties of these responsive films will be crucial in controlling the response amplitudes and speed of the programmed photoinduced shape changes, which are important if these materials are to find practical applications.

In this paper, we report on a remotely controlled magnetic and light-responsive grasping device inspired by the macroscopic design of a chameleon's grasping feet,[36] which are not only soft in nature, but allow the animal to grasp objects in a pincer-like manner. We introduce a novel magnetic response by integrating a polydimethylsiloxane (PDMS) layer functionalized with magnetic carbonyl iron powder with an LCN actuator containing light-responsive azobenzene dyes. This compartmentalized design does not disrupt liquid crystalline ordering or fabrication and allows for the untethered motion, rotation, and transport of the gripper. This differentiates this gripper from other actuators in which movement is usually restricted to one degree of freedom. The azobenzene derivative used to achieve light responsivity is a commonly used chromophore in liquid crystal actuators. We reveal that the actuation rate and displacement are fully determined by the photothermal effect; that is, the photoexcitation of the azobenzene dyes simultaneously results in thermal energy release and photosoftening, which lowers the glass transition of the LCN.

2. Results and Discussion

2.1. Actuator Fabrication

The photoresponsive component of the soft robotic gripper is a splay-aligned LC network consisting of two monomers **1**

and **2**, and a photoresponsive azobenzene derivative **3** with fast *cis*-to-*trans* thermal relaxation (**Figure 1**C).[37] Azobenzene derivatives are used due to their compatibility with the liquid crystal mesogens, showing negligible disruption of the molecular alignment in the polymer network. The splay orientation in LCNs displays uniform and well-controlled photothermal bending deformations, with a higher magnitude of actuation when compared to other alignment configurations, such as antiparallel and homeotropic alignments.[18,23] A splay configuration utilizes the anisotropy of LC molecules and opposing expansion coefficients on opposite surfaces of the film to maximize deformation. The LC monomers used in this work are polymerized at 80 °C in glass cells glued together using 20 µm spacers coated with rubbed planar and unrubbed homeotropic polyimide alignment layers; the resulting freestanding LCN films have a glass transition temperature at $T_g = 83$ °C and storage modulus (in the direction parallel to the planar alignment) of 1.5 GPa at room temperature; detailed preparation procedures are found in the "Experimental Section." Due to the elevated polymerization temperature, anisotropic molar volume shrinkage occurs upon cooling the LCN sample to room temperature due to an increase of molecular order; therefore, the films have a bent shape at room temperature, with the homeotropic surface found on the inside of the curvature. Upon increasing temperature, constructive effects of the coefficients of thermal expansion (CTEs) on opposing surfaces cause the films to return to their original flat shape (Figure S1, Supporting Information). The magnetically functionalized PDMS composite is obtained through manual mixing of a two-component PDMS polymer with carbonyl iron powder in a 1:1 weight ratio. PDMS is chosen as the soft polymer matrix for the magnetic composite due to its low storage modulus, commercial availability, and facile mixing with other functional particles. After degassing the mixture, PDMS(Fe)/LCN bilayers are fabricated by blade coating the uncured PDMS composite onto the photopolymerized LCN film; curing of the PDMS is performed at 100 °C for 2 h. The coating procedure results in adhered layers, with no signs of delamination after several actuation cycles. The magnetic PDMS is coated on the central area of the homeotropic surface of the splay-aligned LC film and is 120 µm
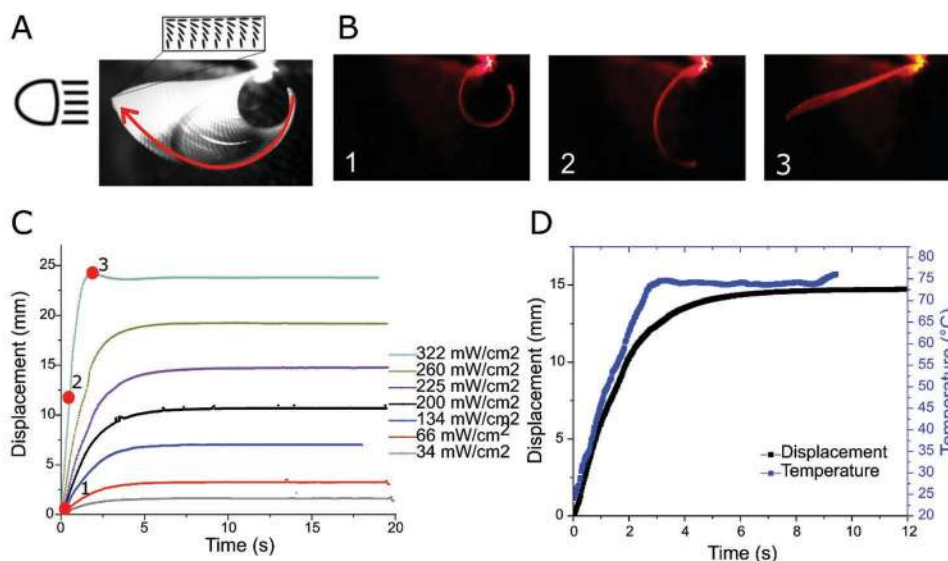
1801643 (2 of 8)

**ADVANCED
SCIENCE NEWS**

www.advancedsciencenews.com

**ADVANCED
OPTICAL
MATERIALS**

www.advopticalmat.de

Figure 2. A) Schematic diagram of the setup used for filming the actuator deformation, in which the LED light is incident on the planar side of the polymer film (16 mm in length), and deformation is directed toward the light source. The image is constructed by overlaying images for the maximum deformation of the LCN when illuminated; the arrow shows the direction of actuation. B) Video snapshots recording different moments of actuation during maximum intensity illumination. Snapshot 1 is the state of rest. C) Endpoint displacement evolution plot for liquid crystalline film as a response to light of varied energy intensities; the numbers refer to the corresponding images in panel (B). D) Time evolution of displacement and temperature increase of LCN when illuminated by light of 225 mW cm^{-2}.

in thickness, Figure 1A. As the magnetic PDMS is coated solely on the middle section of the LCN, it is not directly exposed to incident light used for opening/closing of the soft robot and hence does not influence the light-responsive behavior. Full coverage of the LCN by a PDMS layer has consequences for the photo actuation of the material, for a detailed study we refer to our other work in this issue.[38]

2.2. Light-Responsive Actuation of LCN Single Films

First, the light-responsive behavior of the freestanding LCN films was studied in detail to further understand the underlying causes of photoactuation and to determine the degree of bending and bending rates. The endpoint (tip) position of the film was tracked over time at different incident illumination energy intensities. Concurrently to the tip displacement, the temperature evolution of the film was recorded with a high-speed thermal camera. The actuation analysis was carried out with film deformation and temperature tracking on the sub-second timescale. This time-resolution displacement tracking was achieved by analyzing the film's respective position in all image frames from the actuation videos. Additionally, a fully controlled setup was used in which influence of air flow was minimized by performing the experiments within a sealed glass compartment (Figure S2, Supporting Information) and a detailed description of the setup is found in the Experimental Section.

Upon illumination with a 455 nm light-emitting diode (LED) (corresponding to the azobenzene derivative's absorption peak; Figure S3, Supporting Information), the LCN actuator uncurls and deforms, eventually bending toward the light source (**Figure 2**A,B). Changing the light energy incident on

the LCN results in clear changes in the physical displacement during the initial seconds of actuation, providing information on the rate of actuation and on the differing maximum equilibrium displacements at different incident energies (Figure 2C). Both rate and maximum equilibrium displacements increase with increasing light intensity exposure. Once the lamp is turned off, the LCN relaxes back to its equilibrium shape (Figure S4, Supporting Information), showing reversible actuation.

2.2.1. Rate of Actuation

Upon illumination, the azobenzene derivative in the LCN absorbs incident light which leads to the fast isomerization of the azobenzene derivative and, subsequently, also in heat generation as the *cis*-azo isomer immediately returns to its *trans* configuration.[37] At first, a steady increase of the maximum film temperature with exposure time is recorded and, due to the balance between heat generation by the *cis*-to-*trans* isomerization of the azobenzene molecule and radiation of heat to the environment, the temperature eventually levels off, as seen in Figure 2D. The same time progression observations are evident in the displacement evolution of the LCN, with a clear correlation between increase of film temperature and displacement timescales: one such evolution for 225 mW cm^{-2} light illumination is shown in Figure 2D. Further investigation of interrelated timescales between heating and displacement rates for multiple incident light intensities results in an overall direct correlation between the sample heating rate and the initial actuation rate of the liquid crystal film; see **Figure 3**A. This direct correlation between temperature and displacement highlights the explicit impact of constructive thermal expansions on the opposing surfaces of the splay-aligned LC film
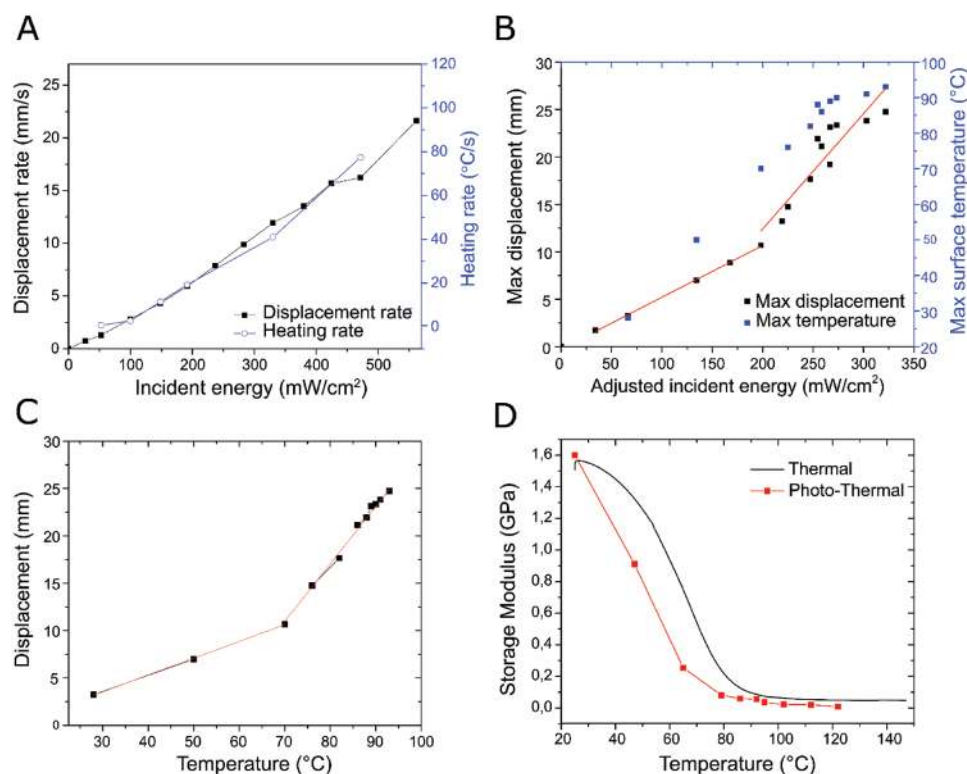
ADVANCED
SCIENCE NEWS
www.advancedsciencenews.com

ADVANCED
OPTICAL
MATERIALS
www.advopticalmat.de

Figure 3. A) Displacement and heating rates for the light triggered actuation of the LCN at different incident light intensities. B) Maximum endpoint displacement and maximum temperature of LCN at equilibrium displacement for varying illumination intensities. C) Maximum endpoint displacement of the LC film tip over the maximum surface temperature of the film during light triggered actuation. Individual points are generated through actuation with varying light intensities. The graph displays a relationship with two linear regions, in which the change in linear slope is observed around 70 °C. D) Dynamic mechanical analysis of the LCN while heated in an oven in the dark (black line) and while illuminated with 455 nm LED light. For the experiments conducted with illumination, individual points are obtained through exposure of the film to different light intensities.

on the macroscopic deformation of the system, revealing that the thermal effect arising from light-responsive behavior in LCNs is the decisive factor in the rate of actuation.

2.2.2. Maximum Endpoint Displacement

The magnitude of maximum deformation at equilibrium caused by light illumination is dependent on the incident light energy (Figures 2D and 3B), and a direct relationship between absorbed energy and maximum temperature is observed. The measured maximum surface temperature of the LCN increases linearly with increasing incident energy (Figure 3B). The relationship between maximum sample temperature at equilibrium and the incident energy can also be represented by a heat balance. Considering P_{absorb} to be the total heat absorbed by the LCN and P_{cool} the convective heat loss to the surroundings, the following simplified heat balance can be set up

$$P_{heat} = P_{absorb} - P_{cool} \qquad (1)$$

In equilibrium, no more heating takes place, so

$$P_{absorb} = P_{cool} \qquad (2)$$

considering the convective heat loss as $P_{cool} = 2hA(T_{max} - T_0)$, with A being the surface area of the film (we assume the heat loss along the edges of the film to be negligible), T_{max} and T_0

the maximum and initial film temperatures, respectively, and h the convective heat transfer coefficient. The equilibrium balance (Equation (2)) can be rewritten

$$T_{max} = T_0 + \frac{P_{absorb}}{h \cdot 2A} \qquad (3)$$

Here we note that T_{max} depends only on the total absorbed energy and the heat lost through the surface of the system, and is independent of thickness if, thickness $\ll$ width and length. Therefore, we see a direct relationship between absorbed energy and maximum temperature attained. In contrast, when the maximum displacement amplitude is plotted against the adjusted incident energy, a bilinear relationship is observed with an inflection point around 200 mW cm^{-2} (Figure 3B). The adjusted incident energy is the light energy corrected for the actual beam exposure at the sample surface (for details, see the Supporting Information). Plotting the displacement against surface temperature of the film more clearly illustrates the two regions; see Figure 3C. The point at which the linearity changes slope is found to be at around 70 °C. The origin for this double linearity in the displacement behavior can be related to the constructive difference in thermal expansion coefficients ($\Delta\alpha$) at the opposing homeotropic and planar aligned surfaces ($\Delta\alpha = \alpha_\perp - \alpha_\parallel$). Plotting $\Delta\alpha$ as a function of temperature, Figure S5 (Supporting Information), reveals the bilinearity

**ADVANCED
SCIENCE NEWS**
www.advancedsciencenews.com

**ADVANCED
OPTICAL
MATERIALS**
www.advopticalmat.de

in the thermal expansion behavior of the polymer, in which the material's glass transition temperature, T_g, corresponds to the temperature at which the change in slope is found.[23,39] The mismatch between the inflection point in the displacement plot (Figure 3C) and the T_g (Figure S5, Supporting Information) is about 15 °C. The fact that the apparent T_g shifts when a sample is illuminated has been previously described as the "photosoftening" effect, that is, the light-induced isomerization of the azobenzene and its corresponding molecular motion is causing softening of the polymer film.[30,31] The photosoftening effect is visualized by performing dynamic mechanical thermal analysis (DMTA) while the sample is illuminated (455 nm) at different light intensities. At each light intensity, the film temperature is recorded with an infrared camera, and the storage modulus is measured. The storage modulus curves for the illuminated sample as well as a regular mechanical analysis with a temperature sweep of the LCN in an unlit oven are compared in Figure 3D. The modulus profile for the illuminated sample does not overlap with a thermal sweep of an unlit sample. The plot for an illuminated sample is shifted toward lower temperatures; the mismatch in the curves is of ≈15 °C and is consistently observed for several films analyzed. Therefore, congruently with the mismatch observed for the inflection point in the displacement plot and the CTE graph (Figure 3C; Figure S5, Supporting Information) of around 15 °C, the mechanical analysis curves (Figure 3D) also display a 15 °C shift.

Based on this detailed analysis, we can conclude that the actuation of the light-responsive LCN appears to be the consequence of photothermal effects: the photoexcitation of the azobenzene dyes, resulting in thermal energy. Temperature appears to be the prevailing factor in the deformation of the LCN, both in setting the rate for actuation and the maximum displacement. The photosoftening effect causes a shift in the apparent T_g of the system, impacting the maximum deformation behavior of the film. With this knowledge, we can accurately control the amplitudes and speed of the photoinduced bending of the soft actuator.

2.3. Remotely Controlled Pick Up, Transport, Rotation, and Release of Cargo

With a detailed understanding of the LCN actuator system, we demonstrate the applicability of stimuli-responsive actuators as a gripper design soft robot. The gripper will employ the photothermal-responsive LCN with a PDMS layer doped with iron powder applied solely in the middle section of the film to achieve localized magnetic response (Figure 1A, vide supra). The magnetic PDMS is not exposed to light; therefore, the photothermal effect leading to open/close actuation is solely due to the light-responsive liquid crystal network. This design allows for the addition of an independent stimulus response (magnetic), while leaving the photoresponsiveness of the device largely free of impediment and with a high degree of control. Light is used to open the gripper, while a simple refrigerator magnet is used to obtain untethered, remote transport, and rotation. This remotely controlled cargo pick up, transport, rotation, and release of the untethered rotational soft robotic gripper is depicted in **Figure 4**A.

In a confined environment, manipulation of the position of the actuator can be remotely controlled within a glass (1 mm thick) compartment through magnetic guidance via the PDMS/Iron layer (Figure 4B; Movie S1, Supporting Information). Once the actuator is brought into the vicinity of a cargo, opening of the device's "arms" is possible with the illumination of the sample ($\lambda = 455$ nm). In our demonstration, the cargo is an asymmetric foam object (5.8 mg) 1.1 times heavier than the gripper device itself. During repetitive cargo pick up and transport tasks, no effects of fatigue of the device were observed. The extent of actuation caused by illumination is directly influenced by the energy supplied to the sample from the LED. This way, the "opening" or pick up mechanism of the soft robot (step (i) in Figure 4A and step (ii) in Figure 4B, respectively) can be remotely steered depending on the size of the cargo to be handled by controlling the intensity of the light stimulus. Furthermore, the rate at which the gripper opens is also influenced by the light energy supplied to the device, with higher incident energies resulting in faster actuation. Once the device is in its opened state above the cargo, switching off the light results in the closing mechanism. Next, locomotion and rotational freedom of the loaded device are possible through magnetic guidance to its destination (step (ii) in Figure 4A). Finally, release of cargo is triggered by illumination which causes the opening of the gripper (step (iii) in Figure 4A and step (iv) in Figure 4B). After release, the device can be transported elsewhere through magnetic guidance. Alternatively, our soft robot could be used to be directly actuated by temperature rather than light, if desired. The gripper can be autonomously opened by changes in local environmental temperature, driving release of the cargo. Such a mechanism in which temperature triggers cargo release is demonstrated in Movie S2 (Supporting Information). An addition versatility of the soft robot gripper is its ability to rotate, allowing for expanded degree of freedom in the gripper's transport movement. The ability to rotate allows the soft robot to be used in tasks that require the additional freedom of moving around corners (Figure S6, Supporting Information) through restricted openings and positioning asymmetric objects in specific orientations (Figure 4C; Movie S3, Supporting Information).

3. Conclusion

We provide a thorough analysis on the photothermal response of an azobenzene-doped liquid crystal actuator by conducting a controlled video and thermal analysis with unprecedented level of detail into temporal temperature effects. These actuators are fully controlled by photoexcitation of the azobenzene dyes resulting in thermal energy governing evolution in both rate and deformation amplitude, connecting these evolutions with mechanical properties and thermal expansion coefficients. We also observe photosoftening of the network and observe its direct impact on the LCNs' actuation performance. Such findings are crucial for making a light-responsive soft actuator with programmed photoinduced shape changes.

Additionally, we demonstrate a novel approach to combine multi-responsive behavior into one device composed of a photothermal-responsive liquid crystal actuator and magnetically functionalized PDMS composite which orchestrates locomotion and rotation via magnetic guidance, allowing for positional control of the actuator even in enclosed spaces and light-driven appendage
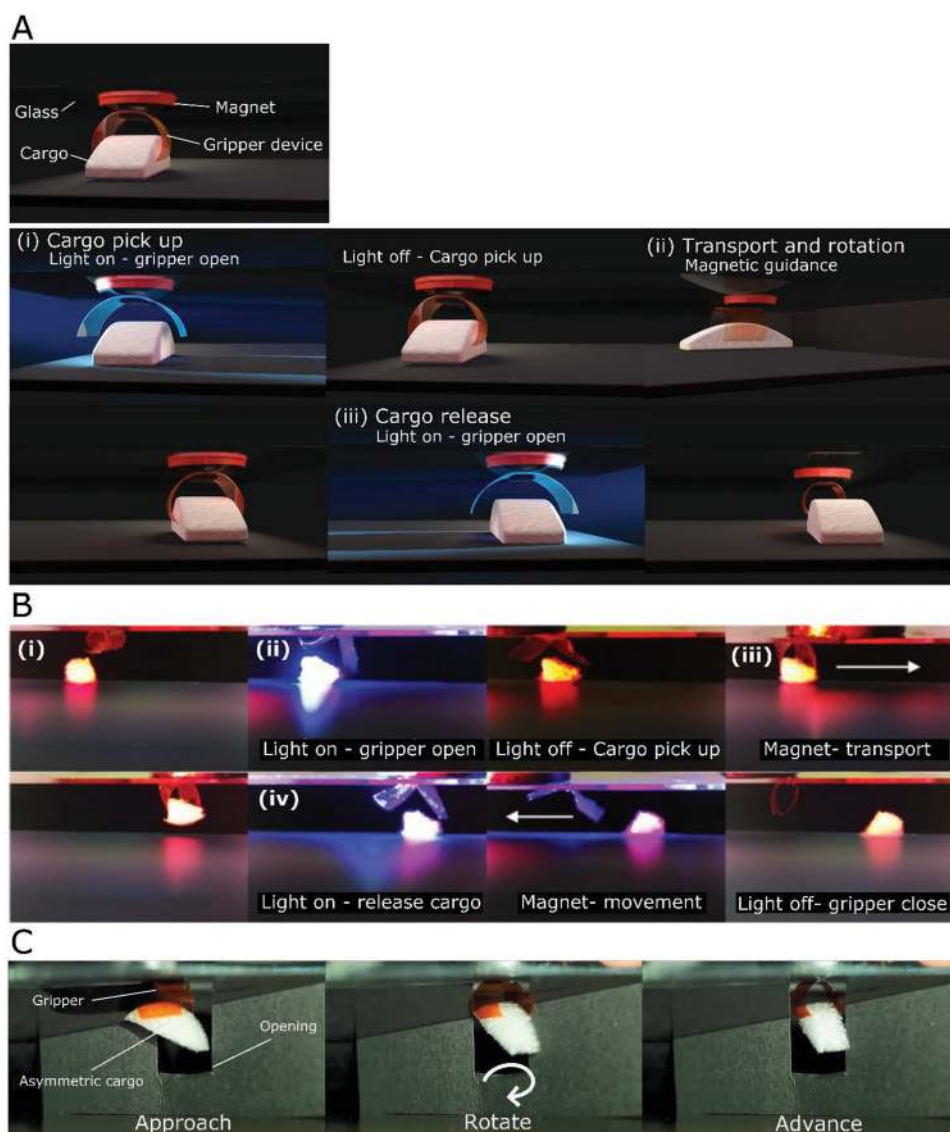
ADVANCED
SCIENCE NEWS
www.advancedsciencenews.com

ADVANCED
OPTICAL
MATERIALS
www.advopticalmat.de

Figure 4. A) Schematic illustration of the cargo pick up, transport, rotation, and release of the untethered rotational soft robotic gripper. B) Snapshots of the untethered pick up, transport, and release of a cargo, performed by the dual-responsive gripper within an enclosed space. C) Snapshots of the soft robot gripper performing the transport of an asymmetric cargo through an opening, which requires rotational motion of the soft robotic gripper.

deformation for manipulation of the soft gripper. Such untethered rotational soft robotic grippers can be used to perform remotely controlled tasks such as cargo pick up, transport, and release and differentiates from other soft robotic grasping devices which typically rely on manual manipulation to perform locomotion.[10–12] Our device architecture will open new routes to fabricate novel untethered multi-responsive soft robotics with programmed bioinspired-responsive functional properties.

4. Experimental Section

Soft Actuator Fabrication: The liquid crystal polymer network was produced by the photocopolymerization of two liquid crystalline monomers (Figure 1B), a monoacrylate, **1** (RM 23; 40.5 mol%, Merck), and a diacrylate, **2** (RM82; 56.5 mol%, Merck), and initiated by a photoinitiator (Irgacure 819, 1 mol%, Ciba). Light responsivity was achieved with the addition of a commercially available azobenzene chromophore with a fast *cis–trans* isomerization, DR1A, **3** (Figure 1B, 2 mol%, Sigma Aldrich). Prior to polymerization, the monomers were dissolved in dichloromethane (DCM) to obtain a homogeneous mixture, and subsequently the solvent was evaporated. Polymerization was carried out in a custom-made glass cell. The glass cells were prepared by gluing together two glass slides; 20 µm diameter glass bead spacers were incorporated into the glue to achieve controlled cell thickness. Prior to cell fabrication, the independent glass slides were coated with polyimide alignment layers; for a splay alignment, one slide contained planar and the other homeotropic alignment layers, Optimer AL 1051 (JSR Micro) and 5661 polyimide (Sunever), respectively. The cells were filled with the LC mixture through capillary action. Cell filling was carried out at 95 °C, at which the LC mixture was isotropic. Subsequently,

the filled cell was cooled to 80 °C, at which temperature the LC mixture is nematic. Photopolymerization of the reactive mesogens was done at this temperature with an Exfo Omnicure S2000 lamp; subsequent thermal treatment at 120 °C for 10 min released thermal stresses arising from polymer shrinkage during polymerization. After polymerization, the cell was opened, and the films were peeled from the glass with razor blades and cut into long strips, in which the alignment direction of the planar side was parallel to the long side of the film.

The magnetically functionalized PDMS composite was obtained through manual mixing of a two-component PDMS polymer (Dow Corning) with carbonyl iron powder (Sigma Aldrich) in a 1:1 weight ratio. After degassing the mixture, PDMS composite/LCN bilayers were fabricated by blade coating the uncured PDMS composite onto the photopolymerized LCN film; curing of the PDMS was performed at 100 °C for 2 h. The PDMS was coated on the homeotropic surface of the splay-aligned LC film and was 120 µm in thickness.

Actuation Analysis of the Liquid Crystal Film: High-speed thermal analysis was performed using a Gobi camera from Xenics. Illumination of the film was performed with a Thorlabs LED lamp, emitting 455 nm light. The setup (Figure S2, Supporting Information) included the blue LED light of 455 nm (Thorlabs M455L3-C2) with a collimation adapter to actuate the samples. Every sample was placed at 9 cm distance from the collimator adapter. A red LED light of 617 nm (Thorlabs LED4D100) at a constant low intensity was used to illuminate the sample in the dark for optimal contrast; this wavelength was outside of the absorption spectrum of the LC films. An LED driver (Thorlabs DC4104) was allowed for alteration of the light energy output. The recording was processed by a Raspberry Pi Model 3B equipped with a Raspberry Pi camera module V2.1 extended with a Fujinon HF25SA-1 camera lens for manually adjustable focus. All samples were placed in such a way that both lights irradiated the sample from the same side (planar surface). A glass box was placed over the sample to prevent airflow influences, also a black velvet cloth was placed behind the sample to enhance the contrast.

Incident Energy Calculation: The integrated sphere measurements determined the total amount of energy provided by the LED light beam to an LC film of 5.3 mm wide. However, the LC film differed in shape when different incident energies were applied. To compare the absolute response for the equilibrium position at each intensity, a correction was applied to approach the correct incident energy over the illuminated surface. There were corrections performed (Figure S7, Supporting Information) for either surface loss due to the sample being in a curled position, surface loss due to the sample being out of the beam, or beam loss due to the sample being in the beam. These features were all determined by analysis of the images.

Mechanical Analysis of the Liquid Crystal Films during Illumination: The mechanical properties of the film were tested with DMTA (Q800 Dynamic Mechanical Analyzer from TA instruments). The analysis was performed to investigate the difference in the material properties of the LCN when heated in an oven or indirectly heated through illumination; similar work was performed in literature.[31] For both illuminated and unlit experiments, the film was clamped at both ends in DMTA clamps, and characterization was performed with a strain-controlled mode. For the unlit measurement, the sample was characterized during a temperature sweep in a closed oven. For the illuminated experiment, the sample temperature was recorded at different incident light intensities with an infrared camera (Gobi from Xenics); the setup for these experiments is shown in Figure S8 (Supporting Information). At each light intensity, the storage modulus was measured and correlated to the sample temperature measured by the infra-red camera.

Supporting Information

Supporting Information is available from the Wiley Online Library or from the author.

Conflict of Interest

The authors declare no conflict of interest.

[1] W. Hu, G. Z. Lum, M. Mastrangeli, M. Sitti, *Nature* **2018**, *554*, 81.

[2] J. Shintake, V. Cacucciolo, D. Floreano, H. Shea, *Adv. Mater.* **2018**, *30*, 1707035.

[3] L. Hines, K. Petersen, G. Z. Lum, M. Sitti, *Adv. Mater.* **2017**, *29*, 1603483.

[4] S. Nocentini, C. Parmeggiani, D. Martella, D. S. Wiersma, *Adv. Opt. Mater.* **2018**, *6*, 1800207.

[5] Y. Xiong, L. Zhang, P. Weis, P. Naumov, S. Wu, *J. Mater. Chem. A* **2018**, *6*, 3361.

[6] J. A. Lv, Y. Liu, J. Wei, E. Chen, L. Qin, Y. Yu, *Nature* **2016**, *537*, 179.

[7] S. I. Rich, R. J. Wood, C. Majidi, *Nat. Electron.* **2018**, *1*, 102.

[8] H. Li, G. Go, S. Y. Ko, J. O. Park, S. Park, *Smart Mater. Struct.* **2016**, *25*, 027001.

[9] J. Mu, C. Hou, B. Zhu, H. Wang, Y. Li, Q. Zhang, *Sci. Rep.* **2015**, *5*, 9503.

[10] O. M. Wani, H. Zeng, A. Priimagi, *Nat. Commun.* **2017**, *8*, 15546.

[11] H. Shahsavan, S. M. Salili, A. Jákli, B. Zhao, *Adv. Mater.* **2017**, *29*, 1604021.

[12] H. Lim, T. Park, J. Na, C. Park, B. Kim, E. Kim, *NPG Asia Mater.* **2017**, *9*, e399.

[13] L. Gao, G. Guo, M. Liu, Z. Tang, L. Xie, Y. Huo, *RSC Adv.* **2017**, *7*, 40005.

[14] C. Huang, J. A. Lv, X. Tian, Y. Wang, J. Liu, Y. Yu, *Smart Mater. Struct.* **2016**, *25*, 095009.

[15] D. Martella, S. Nocentini, D. Nuzhdin, C. Parmeggiani, D. S. Wiersma, *Adv. Mater.* **2017**, *29*, 1704047.

[16] H. K. Bisoyi, A. M. Urbas, Q. Li, *Adv. Opt. Mater.* **2018**, *6*, 1800458.

[17] M. López-Valdeolivas, D. Liu, D. J. Broer, C. Sánchez-Somolinos, *Macromol. Rapid Commun.* **2018**, *39*, 1700710.

[18] C. L. Van Oosten, K. D. Harris, C. W. M. Bastiaansen, D. J. Broer, *Eur. Phys. J. E* **2007**, *23*, 329.

[19] Y. Yu, M. Nakano, T. Ikeda, *Nature* **2003**, *425*, 145.

[20] K. D. Harris, R. Cuypers, P. Scheibe, C. L. van Oosten, C. W. M. Bastiaansen, J. Lub, D. J. Broer, *J. Mater. Chem.* **2005**, *15*, 5043.

[21] S. J. Aßhoff, F. Lancia, S. Iamsaard, B. Matt, T. Kudernac, S. P. Fletcher, N. Katsonis, *Angew. Chem., Int. Ed.* **2017**, *56*, 3261.

[22] Z. Cheng, T. Wang, X. Li, Y. Zhang, H. Yu, *ACS Appl. Mater. Interfaces* **2015**, *7*, 27494.

[23] G. N. Mol, K. D. Harris, C. W. M. Bastiaansen, D. J. Broer, *Adv. Funct. Mater.* **2005**, *15*, 1155.

[24] L. T. De Haan, J. M. N. Verjans, D. J. Broer, C. W. M. Bastiaansen, A. P. H. J. Schenning, *J. Am. Chem. Soc.* **2014**, *136*, 10585.

[25] A. Ryabchun, F. Lancia, A.-D. Nguindjel, N. Katsonis, *Soft Matter* **2017**, *13*, 8070.

[26] S. Herrera-Posada, C. Mora-Navarro, P. Ortiz-Bermudez, M. Torres-Lugo, K. M. McElhinny, P. G. Evans, B. O. Calcagno, A. Acevedo, *Mater. Sci. Eng., C* **2016**, *65*, 369.

[27] M. Winkler, A. Kaiser, S. Krause, H. Finkelmann, A. M. Schmidt, *Macromol. Symp.* **2010**, *291–292*, 186.

[28] T. J. White, D. J. Broer, *Nat. Mater.* **2015**, *14*, 1087.

[29] J. M. Harrison, D. Goldbaum, T. C. Corkery, C. J. Barrett, R. R. Chromik, *J. Mater. Chem. C* **2015**, *3*, 995.

[30] J. Vapaavuori, A. Laventure, C. G. Bazuin, O. Lebel, C. Pellerin, *J. Am. Chem. Soc.* **2015**, *137*, 13510.

[31] K. Kumar, A. P. H. J. Schenning, D. J. Broer, D. Liu, *Soft Matter* **2016**, *12*, 3196.

[32] A. Shimamura, A. Priimagi, J. Mamiya, T. Ikeda, Y. Yu, C. J. Barrett, A. Shishido, *ACS Appl. Mater. Interfaces* **2011**, *3*, 4190.

[33] A. H. Gelebart, G. Vantomme, E. W. Meijer, D. J. Broer, *Adv. Mater.* **2017**, *29*, 1606712.

[34] K. M. Lee, H. Koerner, R. A. Vaia, T. J. Bunning, T. J. White, *Macromolecules* **2010**, *43*, 8185.

[35] Z. Cheng, Y. Zhang, S. Huang, Y. Chen, H. Yu, *Macromolecules* **2017**, *50*, 8317.

[36] M. Spinner, G. Westhoff, S. N. Gorb, *Sci. Rep.* **2014**, *4*, 12.

[37] A. H. Gelebart, D. J. Mulder, M. Varga, A. Konya, G. Vantomme, E. W. Meijer, R. L. B. Selinger, D. J. Broer, *Nature* **2017**, *546*, 632.

[38] M. Pilz da Cunha, Y. Foelen, T. A. P. Engels, K. Papamichou, M. Hagenbeek, M. G. Debije, A. P. H. J. Schenning, *Adv. Opt. Mater.* **2019**, *7*, 1801604 (this issue).

[39] J. J. Wie, K. M. Lee, T. H. Ware, T. J. White, *Macromolecules* **2015**, *48*, 1087.

1801643 (8 of 8)